



A theoretical model for calculation of the detective quantum efficiency in granular scintillators

D. Cavouras^{a,*}, I. Kandarakis^a, S. Tsoukos^b, A. Kateris^b, C.D. Nomicos^c,
G.S. Panayiotakis^b

^aDepartment of Medical Instrumentation Technology, Technological Educational Institution of Athens, Ag. Spyridonos, Aigaleo, 122 10 Athens, Greece

^bDepartment of Medical Physics, Medical School, University of Patras, 265 00 Patras, Greece

^cDepartment of Electronics, Technological Educational Institution of Athens, Ag. Spyridonos, Aigaleo, 122 10 Athens, Greece

Received 13 April 2001; received in revised form 3 July 2001; accepted 8 July 2001

Abstract

A theoretical model has been developed for calculating the detective quantum efficiency (DQE) of scintillators, by taking into account the internal structure of granular scintillators often used in medical imaging detectors. Scintillators were considered to consist of N elementary thin layers containing spherical scintillating grains of equal size. Grains were assumed to be regularly distributed within each thin layer, the thickness of the latter being equal to the grain diameter. Values of the X-ray absorption and X-ray attenuation coefficients, of the intrinsic X-ray to light conversion efficiency and of the optical scattering and absorption coefficients were used as input data to the model. Optical scattering and optical absorption coefficients were determined by fitting the model to experimental luminescence data. The model was employed to calculate the detective quantum efficiency of $\text{La}_2\text{O}_2\text{S:Tb}$, $\text{Y}_2\text{O}_2\text{S:Tb}$, $\text{Y}_2\text{O}_2\text{S:Eu}$, ZnSCdS:Ag , ZnSCdS:Au,Cu scintillators. Results of the calculations were found close to values published in previous studies. © 2001 Elsevier Science Ltd. All rights reserved.

Keywords: Scintillators; X-ray imaging; Phosphor screens; DQE

1. Introduction

Scintillators are incorporated in radiation detectors employed in a large variety of applications (nuclear and particle physics, biomedical imaging, astrophysics, crystallography, industrial research etc.). These detectors are either used for simple detection of ionizing radiation or for imaging radiating objects. Depending on the preparation technique, scintillators are either of compact form or of granular form. In the latter case the active scintillating material consists of grains embedded in a non-active binding material (Ludwig, 1971; Arnold, 1979; Curry et al., 1990; Giakoumakis et al., 1991; Yaffe and Rowlands, 1997; Lindström and Carlsson, 1999). Due to this structure, optical quanta generated within the active material may be scattered by the grains. Consequently, light is significantly attenuated inside the scintillator before emission from its outer surface. This affects the efficiency of a detector to accurately register the spatial distribution of impinging radiation quanta.

The detection and imaging performance of scintillators may be assessed by various parameters expressing either the quantity or the quality of the output signal as well as the level of quantum noise (Swank, 1972; Dick and Motz, 1981; Shaw and Van Metter, 1984; Bunch et al., 1987). Output signal and noise of detectors are often described in

*Corresponding author at: 37–39 Esperidon Street, 17671 Kallithea, Athens, Greece. Tel.: +30-1-5385-372; fax: +30-1-9594-558.
E-mail address: cavouras@hol.gr (D. Cavouras).

combination, by one single parameter, the signal to noise ratio (SNR). SNR is usually evaluated via the detective quantum efficiency (DQE). DQE expresses the efficiency of a detector to transfer both signal and noise from the input to the output and it is defined as the square of the ratio of the output SNR and the input SNR. Thus DQE may be considered as a parameter describing the overall performance of a detector.

DQE has been previously experimentally and theoretically evaluated using either laborious and delicate experimental techniques (Dick and Motz, 1981; Bunch et al., 1987; Ginzbourg and Dick, 1993; Kandarakis et al., 1996) or calculations that do not give emphasis to the presence of grains (Tapiovaara and Wagner, 1985; Sandborg and Carlsson, 1992). Grains have only been included in theoretical models for calculation of the absolute efficiency of scintillating phosphor screens (Giakoumakis et al., 1991; Lindström and Carlsson, 1999). In the present study a theoretical model for DQE calculation, that takes into account the granular structure of the scintillator as well as the scattering, absorption and reflectivity effects, is described. This model may be used to calculate and predict the DQE of scintillators exhibiting optical self-scattering and self-absorption properties.

2. Method

2.1. Definition of the detective quantum efficiency

The detective quantum efficiency, η_D , has been defined (Dainty and Shaw, 1974) by the ratio:

$$\eta_D(E, L_0) = [\text{SNR}_0(E, L_0)/\text{SNR}_1]^2 \quad (1)$$

where SNR_0 , SNR_1 , signify output and input signal to noise ratio respectively. E is the energy of the incident X-ray quanta and L_0 is the thickness of the scintillator.

2.2. Input signal to noise ratio

The input signal to an imaging detector is often expressed by the incident X-ray quantum fluence (number of quanta per unit of area). However, in many cases imaging detectors are operated as energy integrating, and not as photon counting systems (Swank, 1972; Sandborg and Carlsson, 1992; Williams et al., 1999). Energy integration yields an output signal proportional to the total energy (number of photons times the energy of one photon) deposited within the detector. This is especially important for polyenergetic incident X-ray beams, where, depending on spectral energy value, equal numbers of incident X-ray quanta may result in unequal energy depositions in the detector. Thus, the incident X-ray energy fluence, rather than quantum fluence, should be taken into account in input signal calculations. On the other hand, input noise has been expressed by the Poisson standard deviation of the X-ray quantum fluence weighted by photon energy E (Williams et al., 1999). Thus the input signal to noise ratio may be written as:

$$\text{SNR}_{\text{IN}} = \frac{\int_0^{E_0} [d\bar{\Phi}_Q(E)/dE]E dE}{\left[\int_0^{E_0} [d\bar{\Phi}_Q(E)/dE]E^2 dE \right]^{1/2}} \quad (2)$$

where E is the energy of one X-ray quantum. E_0 is the maximum energy of the spectrum of X-rays. $[d\bar{\Phi}_Q(E)/dE]$ is the mean differential X-ray quantum fluence spectral distribution (X-ray quantum fluence per energy interval dE) averaged over the detector surface. This distribution has been previously theoretically described (Storm, 1972; Tucker et al., 1991; Tan and Heaton, 1994) and calculated in terms of X-ray source characteristics. The numerator of (2) may be considered as the first statistical moment (Swank, 1973) of this distribution and expresses the total X-ray energy incident on the scintillator. This quantity corresponds to the input signal. The denominator is the square root of the Poisson variance of $[d\bar{\Phi}_Q(E)/dE]$ weighted by the X-ray energy. This may be considered as the second moment of the energy distribution and expresses noise.

If the incident radiation is monoenergetic then simply the X-ray quantum fluence may be used as input signal. In this case the Poisson standard deviation is given as the square root of the fluence. Hence the input SNR is given by the square root of the fluence $\bar{\Phi}_Q$.

2.3. The total output optical signal of the scintillator

In the present study the scintillator is considered as a fluorescent layer of total thickness $L = L_0$, consisting of a number (N) of thin layers containing scintillating grains of equal size (Fig. 1). In real granular scintillators, grains of various sizes are randomly distributed. However, according to the efficiency equivalence principle (Lindström and Carlsson, 1999), the light fluence emitted by a real scintillator will be equal to the fluence of an ideal scintillator

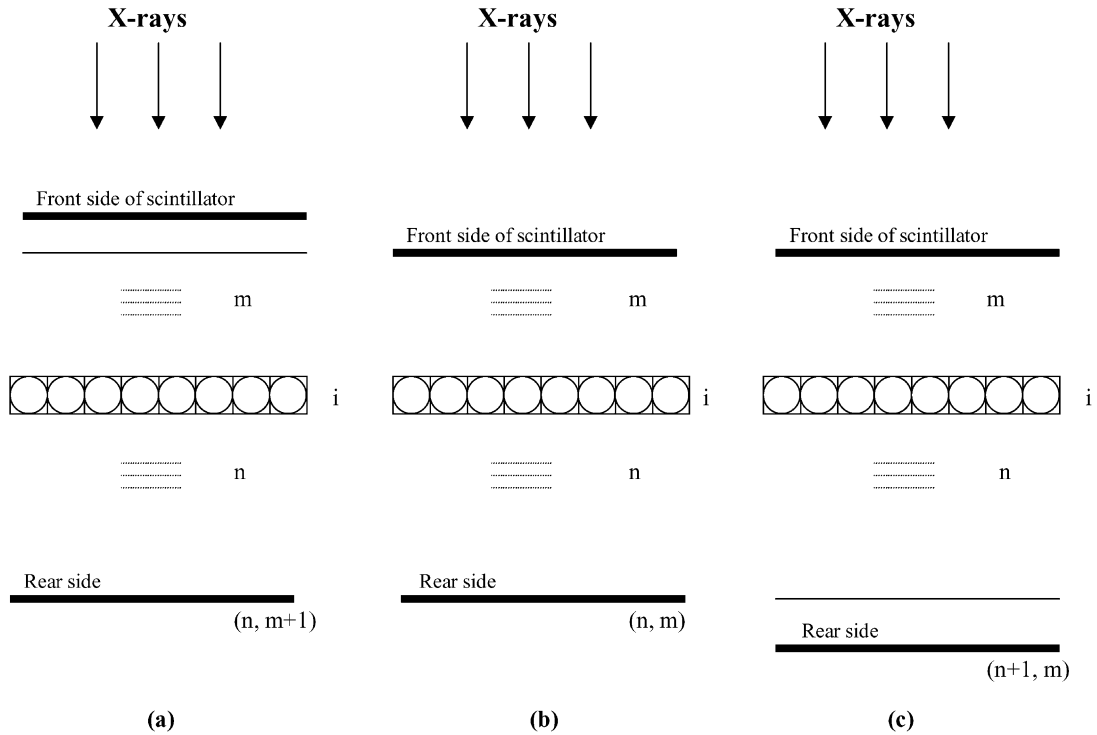


Fig. 1. Cross section of the scintillator layer.

containing regularly distributed grains of identical shape and size. In this model the size was considered equal to the mean size of the real scintillator grains. The grains were simulated by spherical particles, The thickness dL of each thin layer was assumed to be equal to the particle diameter. The gap between grains was considered to be filled with binding material and air, both causing negligible attenuation to the incident radiation. Hence the mass of a spherical scintillating grain may be considered to be homogeneously distributed within an elementary cube of volume $(dL)^3$. Thus the particles could be seen as cubes (Fig. 1) of density lower than that of the spherical particles. This density was assumed to be decreased by a factor equal to the ratio of the corresponding volumes (sphere volume over cube volume). X-rays (or γ -rays) were assumed to fall perpendicularly with respect to the scintillator front surface at $(L = 0)$.

The output signal, $\Phi_A(E, L_0)$ of the scintillator may be expressed by the equation

$$\bar{\Phi}_A(E, L_0) = \bar{\Phi}_Q(E) \bar{\eta}_Q^T(E, L_0) \sum_{i=0}^N \bar{\eta}_Q^R(E, L_i) \bar{\Phi}_A(L_i) \quad (3)$$

$\bar{\Phi}_A$ represents the total number of optical quanta emitted by the scintillator. $\bar{\Phi}_Q$ is the incident X-ray quantum fluence (photons per unit of area) considered to be averaged over the detector surface. L_0 is the total thickness of the scintillator. $\bar{\eta}_Q^T$ is the total quantum absorption efficiency expressing the probability of X-ray absorption within the whole scintillator mass. $\bar{\eta}_Q^R(E, L_i)$ is the relative quantum absorption efficiency, which is a function giving the probability for an absorbed X-ray quantum of energy E to interact in a layer L_i , at depth $L = idL$, $i = 1, 2, 3, \dots, N$. $\bar{\Phi}_A(L_i)$ is the number of optical quanta generated at the depth L_i , that escape out of the scintillator, after an X-ray interaction at this depth. All quantities described in Eq. (3) are considered to be averaged over the area of the detector. In the case of polyenergetic beams Eq. (3) must be integrated over the spectrum of X-rays.

2.4. Quantum absorption efficiency ($\bar{\eta}_Q^T$) and relative absorption probability ($\bar{\eta}_Q^R$)

Total quantum absorption efficiency may be given by the sum of X-ray absorption contributions from all thin scintillator layers, as follows:

$$\bar{\eta}_Q^T(E, L_0) = \frac{[\mu_{cn}(E)/\rho]}{[\mu_T(E)/\rho]} \sum_{i=1}^N \{ \exp[-(\mu_T(E)/\rho)(i-1)\rho_L dL] - \exp[-(\mu_T(E)/\rho)i\rho_L dL] \} \quad (4)$$

where $\mu_{\text{en}}(E)/\rho$ is the X-ray energy mass absorption coefficient, $\mu_{\text{T}}(E)/\rho$ is the X-ray total mass attenuation coefficient. ρ_{L} is the packing density (pure scintillator mass per unit of layer volume). The first exponential term in (4) gives the fraction of X-ray fluence incident on the i th layer after being transmitted and attenuated through $(i-1)$ thin layers. The second exponential term expresses attenuation from i layers, e.g. including the contribution from the i th layer. The subtraction of the two exponential terms gives the X-ray attenuation within the i th layer. The ratio $[\mu_{\text{en}}(E)/\rho]/[\mu_{\text{T}}(E)/\rho]$ of the two X-ray coefficients expresses the fraction of absorbed X-ray energy with respect to the totally attenuated energy.

As described previously the relative quantum absorption efficiency $\bar{\eta}_{\text{Q}}^{\text{R}}(E, L_i)$ is a distribution function expressing the probability of an already absorbed X-ray quantum to deposit its energy at a specific depth L_i , within the scintillator. $\bar{\eta}_{\text{T}}^{\text{R}}$ is given as the relative absorption probability by the formula:

$$\bar{\eta}_{\text{Q}}^{\text{R}}(E, L_i) = \frac{[\exp[-(\mu_{\text{T}}(E)/\rho)(i-1)\rho_{\text{L}} dL] - \exp[-(\mu_{\text{T}}(E)/\rho)i\rho_{\text{L}} dL]}{\sum_{i=1}^N [\exp[-(\mu_{\text{T}}(E)/\rho)(i-1)\rho_{\text{L}} dL] - \exp[-(\mu_{\text{T}}(E)/\rho)i\rho_{\text{L}} dL]} \quad (5)$$

The numerator of (5) expresses attenuation within the i th layer, while the denominator expresses total attenuation in the scintillator.

2.5. Optical quanta generated per X-ray absorbed

Optical photons generated at the i th layer at depth $idL = L_i \neq 0$, were considered to be divided into two equal parts: one part propagating towards the front scintillator's surface and the other part propagating towards the rear scintillator side. This configuration assumes one-dimensional light propagation. This assumption has been also made in previous theoretical models for the absolute luminescence efficiency of phosphor screens (Hamaker, 1947; Kubelka, 1948; Ludwig, 1971; Giakoumakis et al., 1991; Lindström and Carlsson, 1999). The optical quanta created at the i th layer, and emitted from the rear scintillator's side after an X-ray absorption, define an optical pulse denoted as $\Phi_{\text{A,B}}^i(n, m)$, where m and n are the numbers of layers in front and behind the i th layer respectively (Fig. 1b). Subscript B denotes back or rear side emission. If a new layer is added behind the rear scintillator side, the optical pulse may be written (Giakoumakis et al., 1991).

$$\Phi_{\text{A,B}}^i(n+1, m) = \Phi_{\text{A,B}}^i(n, m)\exp[-\lambda_{\text{A}} dL]\exp[-\lambda_{\text{S}} dL] \quad (6)$$

where λ_{A} and λ_{S} are the optical absorption and optical scattering coefficients respectively. Exponential factors in (6) express the optical attenuation (absorption and scattering) caused by the new layer on $\Phi_{\text{A,B}}^i(n, m)$. Since the model considers only one-dimensional X-ray and light propagation, the term optical scattering signifies optical photon backscattering towards the opposite direction. On the other hand optical absorption signifies optical photon disappearance.

If that new layer is added on the front surface of the scintillator (Fig. 1a), then the number of optical quanta (optical pulse) emitted from the rear side, is given by:

$$\Phi_{\text{A,B}}^i(n, m+1) = \Phi_{\text{A,B}}^i(n, m) + \Phi_{\text{A,F}}^i(n, m)[1 - \exp[-\lambda_{\text{S}} dL]]\exp[-(\lambda_{\text{S}} + \lambda_{\text{A}})[(m+1) + n] dL] \quad (7)$$

where $\Phi_{\text{A,F}}^i(n, m)$ is the number of optical quanta generated at the i th layer, after absorption of one X-ray quantum, which are directed towards the X-ray beam incidence side and, after traversing through m layers, are emitted by the front scintillator surface. Subscript F in (7) denotes front side emission. The first exponential function in Eq. (7) expresses the fraction of optical photons, directed towards the front surface, which are backscattered from the new $(m+1)$ th layer. The second exponential function describes the attenuation (absorption and scattering) suffered by the optical quanta which are backscattered from the $(m+1)$ th layer and travelling through $[(m+1) + n]$ layers are emitted from the rear side.

Applying Eqs. (6) and (7) in recursion, for $(n-1), (n-2)\dots$ and $(m-1), (m-2)\dots$ layers, it can be shown (see Appendix A) that:

$$\Phi_{\text{A,B}}^i(n, m) = (1 - \rho_0)\Phi_{\text{A,B}}^i(0, 0)[1 + (1 - \exp[-\lambda_{\text{S}} dL]) \sum_{k=0}^{m-1} \exp[-(\lambda_{\text{A}} + \lambda_{\text{S}})(2k+1) dL]]\exp[-n(\lambda_{\text{A}} + \lambda_{\text{S}}) dL] \quad (8)$$

where ρ_0 is the fraction of optical quanta reflected backwards from the rear side which is considered to be absorbed within scintillator's mass. Eq. (8) expresses the number of optical quanta generated at the thin layer (i) at depth L per X-ray quantum absorbed, and emitted by the rear side of the scintillator of total thickness $L_0 = NdL = (m+1) + n$ dL. $\Phi_{\text{A,B}}^i(0, 0)$ is the number of optical quanta created in the i th layer within the scintillator, without taking into account the

optical attenuation caused by the other (n and m) layers. This number may be calculated by the equation:

$$\Phi_{A,B}^i(0,0) = \frac{1}{2} \eta_C \left[\frac{E}{hc/\lambda} \right] \tag{9}$$

where η_C is the intrinsic X-ray to light conversion efficiency which expresses the fraction of absorbed X-ray energy converted into light energy within the scintillator's mass. hc/λ is the energy of an optical quantum with λ being the wavelength and c the light velocity. The factor (1/2) denotes that the total flux produced in the i th layer is divided into two equal and opposite directed fluxes.

2.6. The output noise

Output noise is expressed by the standard deviation of the output signal. The square of the noise, that should be used in DQE determination, is expressed by the corresponding variance (Swank, 1972; Dick and Motz, 1981; Shaw and Van Metter, 1984; Tapiovaara and Wagner, 1985; Sandborg and Carlsson, 1992). This variance may be expressed as follows (see Appendix).

$$\begin{aligned} \text{var}[\Phi_A(E, L_0)] &= \bar{\Phi}_Q^{\text{ABS}}(E) \text{var}[\Phi_A^X(E, L_0)] + \overline{\Phi_A^{X^2}}(E, L_0) \text{var}[\Phi_Q^{\text{ABS}}(E)] \\ &= \bar{\Phi}_Q^{\text{ABS}}(E) [\overline{\Phi_A^{X^2}}(E, L_0)] \end{aligned} \tag{10}$$

where

$$\bar{\Phi}_Q^{\text{ABS}}(E) = \bar{\Phi}_Q(E) \bar{\eta}_Q^{\text{T}}(E, L_0) \tag{11}$$

is the mean X-ray quantum fluence absorbed by the scintillator of total thickness $L_0 = NdL$.

$$\Phi_A^X(E, L_0) = \sum_{i=0}^N \bar{\eta}_Q^{\text{R}}(E, L_i) \bar{\Phi}_A(L_i) \tag{12}$$

is the mean number of optical quanta emitted by the scintillator of total thickness L_0 , per X-ray quantum absorbed. $\overline{\Phi_A^{X^2}}(E, L_0)$ is the mean number of the squares of optical quanta created at various depths L , and emitted by the scintillator of total thickness L_0 per X-ray absorbed. This number is given by:

$$\overline{\Phi_A^{X^2}}(E, L_0) = \sum_{i=0}^N \bar{\eta}_Q^{\text{R}}(E, L_i) [\bar{\Phi}_A(L_i)]^2 \tag{13}$$

Thus the square of the output signal to noise ratio may be expressed by the equation:

$$[\text{SNR}_{\text{OUT}}]^2 = \frac{[\bar{\Phi}_Q(E) \bar{\eta}_Q^{\text{T}}(E, L_0) \sum_{i=0}^N \bar{\eta}_Q^{\text{R}}(E, L_i) \bar{\Phi}_A(L_i)]^2}{\bar{\Phi}_Q(E) \bar{\eta}_Q^{\text{T}}(E, L_0) \sum_{i=0}^N \bar{\eta}_Q^{\text{T}}(E, L_i) [\bar{\Phi}_A(L_i)]^2} \tag{14}$$

The quantities expressed by Eqs. (12) and (13), which appear in the numerator and in the denominator of (14) respectively, correspond to the first and second moments of the pulse height distribution of the emitted optical pulses, as defined by Swank (Swank, 1972, 1973).

2.7. Calculation of the detective quantum efficiency

Using Eqs. (1),(2),(14) and considering $\bar{\Phi}_A(L_i) \equiv \bar{\Phi}_{A,B}^i(n, m)$, as it is given by Eq. (8), the detective quantum efficiency was calculated for various scintillator materials. X-ray energy absorption and X-ray total attenuation coefficients (in Eqs. (4) and (5)) for these materials were calculated using the corresponding coefficients of the chemical elements of the scintillator material, as tabulated by Storm and Israel (Storm and Israel, 1967). Values of the intrinsic X-ray to light energy conversion efficiency η_C , of the reflected fraction ρ , and of the wavelength λ , were obtained from previous studies (Kandarakis et al., 2001; Kandarakis and Cavouras, 2001a,b). The optical scattering and optical absorption coefficients, (λ_S, λ_A), were obtained by fitting calculated optical signal curves to experimental data (Kandarakis and Cavouras, 2001a,b; Cavouras et al., 1998, 2000).

3. Results and discussion

Fig. 2 shows curves expressing the detector optical gain (emitted optical quantum fluence per incident X-ray quantum fluence). Solid lines correspond to theoretical calculations performed by dividing Eq. (3) by the X-ray quantum fluence Φ_Q . Theoretical curves were fitted to experimental data (points) employing the Levenberg–Marquard method (Press et al., 1990). Experimental uncertainties in measured values (points) were of the order of 4–5%. The experimental optical gain values were obtained by exposing to X-rays scintillator layers prepared in laboratory. The optical quantum fluence, Φ_A , was experimentally determined by a photomultiplier (EMI 9558 QB) coupled to an electrometer (Cary 401). X-rays were produced by a tungsten target tube, operated at voltages from 60 to 140 kV. X-ray quantum fluence data were obtained by suitably converting X-ray exposure values measured by an ionization chamber (Johns and Cunningham, 1983). For each scintillator layer best fitting was obtained by allowing parameters λ_A and λ_S , in Eq. (8), to vary. Initial values of these parameters were estimated, from previous studies based on the Hamaker–Ludwig model (Cavouras et al., 1998, 2000; Kandarakis and Cavouras, 2001a,b). Results of the fitting procedure are tabulated in Table 1, which shows coefficient values for various materials. As it is observed: (1) Light attenuation was mainly due to optical scattering and to a lesser extent to optical absorption. This may be explained by considering the presence of grains, which mainly act as light scatterers. (2) Optical scattering coefficient is higher when the mean wavelength of light quanta emitted by the scintillator is lower as it becomes obvious by comparing $Y_2O_2S:Tb$ and $Y_2O_2S:Eu$ scintillators.

The shape and the level of the detector gain curves in Fig. 2 are determined by the X-ray absorption properties of the layer, the conversion of X-rays into light and the optical attenuation within the material. Scintillators exhibiting high density (see Table 1) and high effective atomic number, like La_2O_2S , are efficient X-ray absorbers and show high gain values. Non-efficient X-ray absorption may be counterbalanced by high intrinsic conversion efficiency. This is what happens with $ZnSCdS:Ag$ scintillator. This material shows low X-ray absorption (low effective atomic number). However, due to its high conversion efficiency (0.21) (see Table 1), its optical gain is comparable to that of $La_2O_2S:Tb$ in the range of tube voltages lower than 100 kV which is very useful for medical imaging. On the other hand $ZnSCdS:Ag,Cu$, although with identical X-ray absorption properties with $ZnSCdS:Ag$ it exhibits lower gain due to its lower intrinsic conversion efficiency (0.17) (see Table 1). Low optical attenuation properties may also increase gain. This is the case of $Y_2O_2S:Eu$ scintillator emitting red light, as compared to the green emitting $Y_2O_2S:Tb$. The latter shows higher intrinsic efficiency than $Y_2O_2S:Eu$ (0.18 and 0.12 respectively as shown in Table 1). However, it emits light of

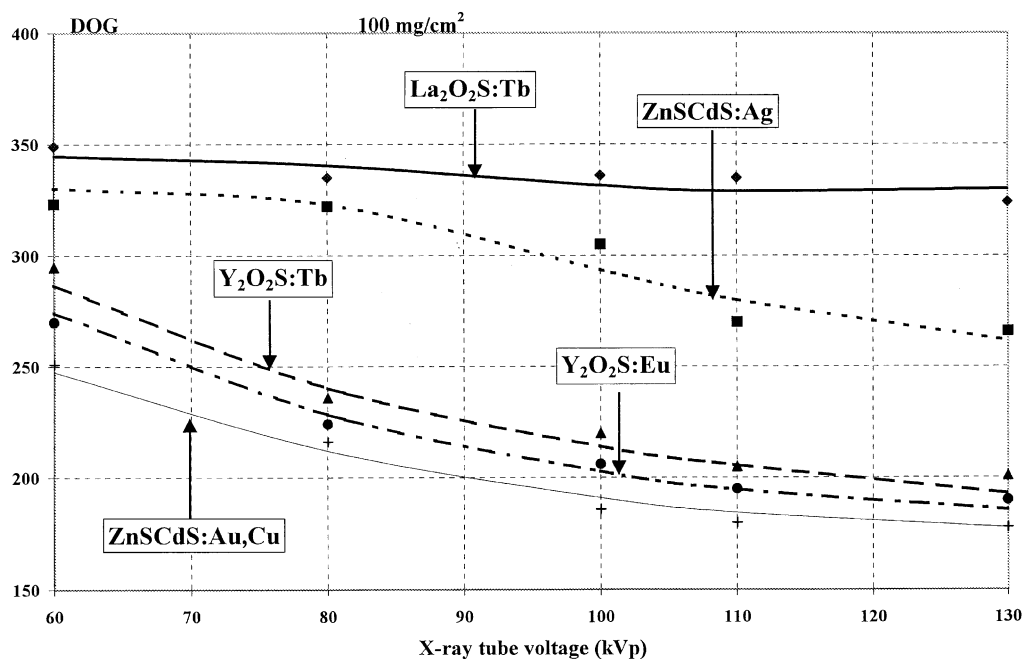


Fig. 2. Detector optical gain (DOG) of various scintillator layers corresponding 100 mg/cm² coating thickness.

Table 1

Values of density (Arnold, 1979; Zweig and Zweig, 1983; Gurvich, 1995), intrinsic conversion efficiency (Kandarakis et al., 1996, 1997a,b, 2001, Cavouras et al., 1997) and optical parameters of the scintillators used in this study

Scintillator	Density (g/cm ³)	Light wavelength (nm)	η_C	λ_A (cm ² /g)	λ_S (cm ² /g)
La ₂ O ₂ S:Tb	5.54	545	0.18	0.9	500
Y ₂ O ₂ S:Tb	4.89	418, 545	0.18	0.9	500
Y ₂ O ₂ S:Eu	4.89	590, 670	0.12	0.45	250
ZnSCdS:Ag	4.43	530	0.21	1.5	380
ZnCdS: Au,Cu	4.43	540	0.17	1.5	400

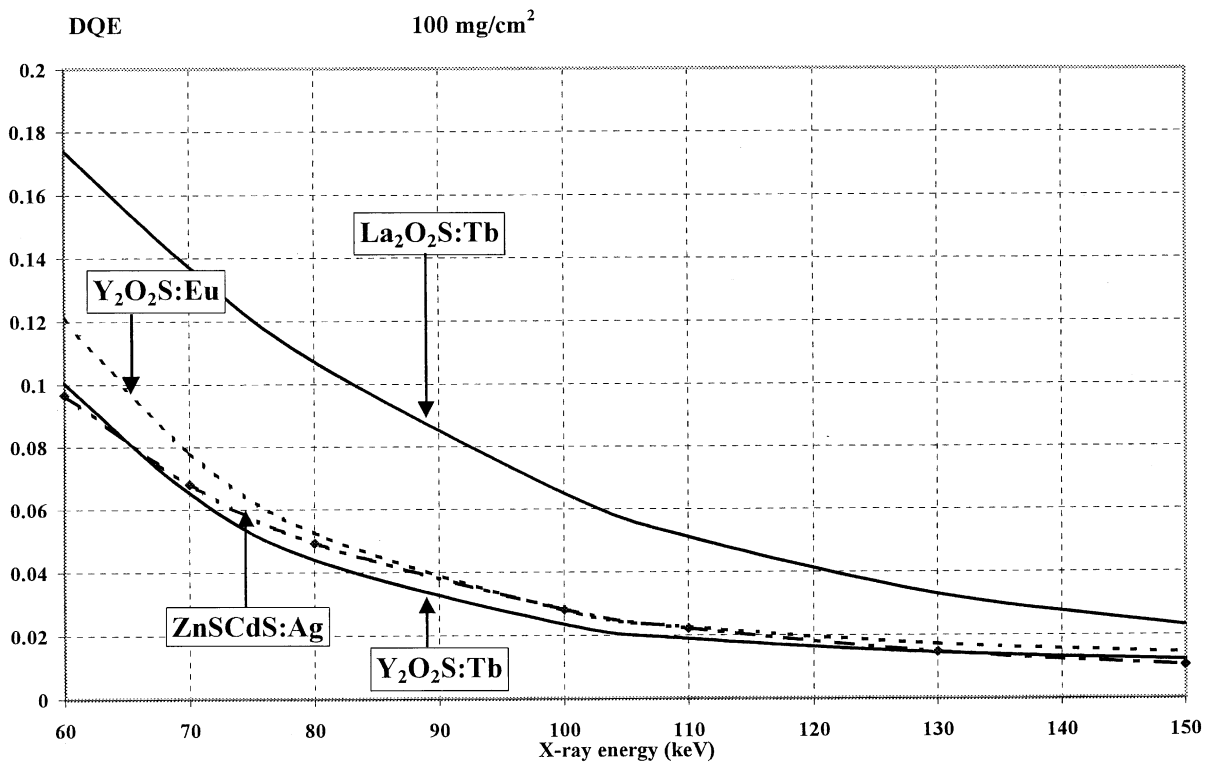


Fig. 3. Variation of calculated detective quantum efficiency as a function of X-ray energy, for various scintillators.

higher frequency and thus it exhibits higher scattering coefficient than Y₂O₂S:Eu. This reduces the output optical signal of Y₂O₂S:Tb resulting in approximately equal optical gain for the two materials.

Fig. 3 shows the variation of calculated DQE curves as a function of X-ray energy for various scintillator materials. DQE is shown to decrease with X-ray energy. Physically this may be explained by considering the increasing X-ray transmission through the scintillator layers as energy increases. This limits the total energy deposited within the active layer mass and reduces the output signal. On the other hand, since energetic X-rays are more penetrating, the sites of X-ray absorption and light production events are distributed along longer X-ray trajectories, e.g. within a larger volume of the scintillator mass. This results in a wider statistical distribution of the sizes of the output optical pulses. Hence output signal variance and quantum noise increases. At higher energies ($E > 130$ keV) DQE values show a slower tendency to decrease and differences between scintillator materials are minimal.

La₂O₂S:Tb exhibits highest DQE values in the whole X-ray energy range under consideration. This is due to the intrinsic physical properties (effective atomic number, material density) of this material. However, due to the terbium activator, La₂O₂S:Tb emits green light corresponding to high light frequencies and hence to a relatively high optical

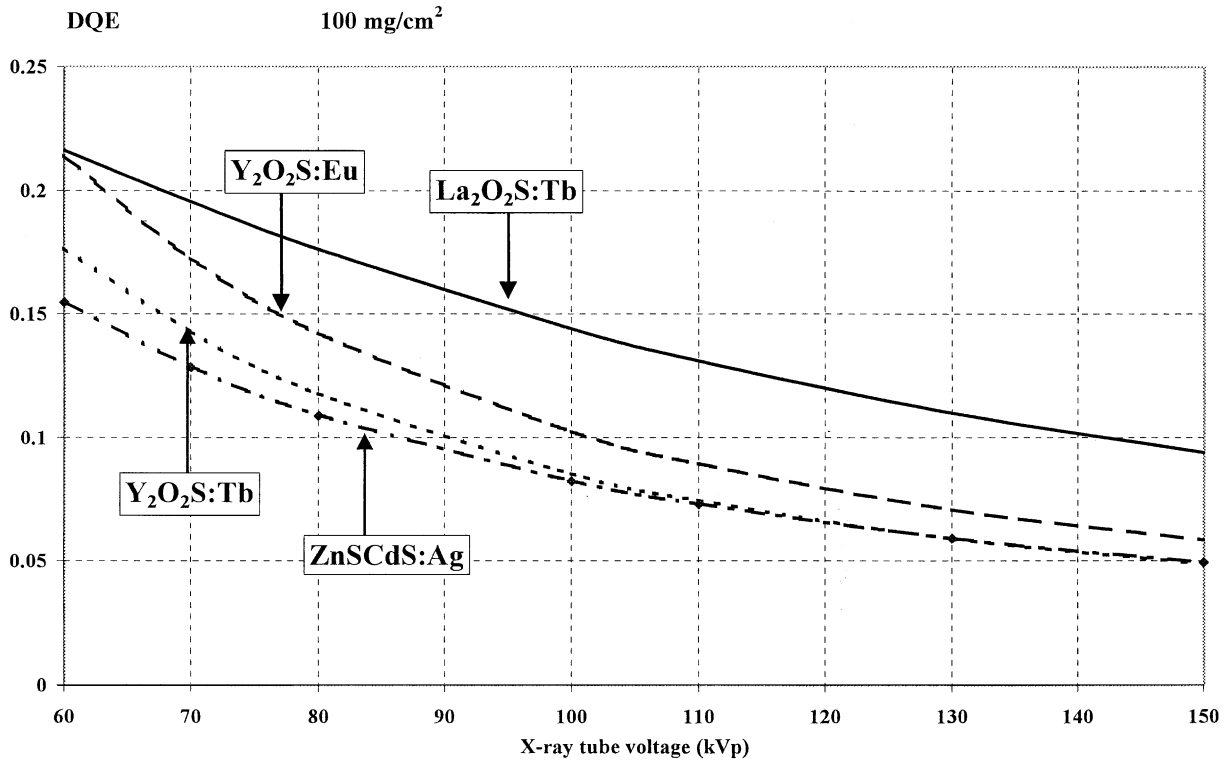


Fig. 4. Variation of calculated detective quantum efficiency as a function of X-ray tube voltage for various scintillators.

scattering coefficient. This should cause a slight decrease in output signal and a corresponding increase in the statistical variance and noise. This may be evident by comparing the corresponding DQE values of $\text{Y}_2\text{O}_2\text{S:Tb}$ and $\text{Y}_2\text{O}_2\text{S:Eu}$. The two scintillators differ only in their activator and emit at different light frequencies. The europium activated material emitting at lower optical frequencies exhibits lower scattering coefficient. $\text{Y}_2\text{O}_2\text{S:Tb}$ emits at higher frequencies, close to those of $\text{La}_2\text{O}_2\text{S:Tb}$, corresponding to higher scattering. This seems to be the principal cause of the slightly higher DQE of $\text{Y}_2\text{O}_2\text{S:Eu}$ with respect to the terbium activated one. The DQE of the ZnSCdS:Ag , Cu scintillator is not shown since it was found practically identical to the corresponding ZnSCdS:Ag curve. This may be explained by considering that the main difference between the two scintillators is the value of the intrinsic conversion efficiency (Table 1), found in both numerator and denominator of SNR_{OUT} (within function Φ_A of Eq. 14). On the other hand, there is only a slight difference in the optical scattering coefficients (Table 1) between the two materials.

Fig. 4 shows DQE curves corresponding to polyenergetic incident X-ray beams, often used in practical situations. The values shown in this figure are affected by the shape of the X-ray energy spectrum employed in the calculations. This spectrum is determined by the high voltage of the X-ray tube, the type of voltage generator, the aluminum filter thickness etc. In our case a three phase high voltage generator and a 2 mm Al X-ray tube filter were used during the optical gain measurements. An additional 20 mm Al filter thickness was also employed to simulate spectrum alteration by the imaged object, e.g. human body intervening between the X-ray source and the detector in medical examinations. The high voltage generator was operated at voltages from 60 to 130 kVp. These values determine the maximum energy of the X-ray spectrum in each case. The corresponding mean X-ray energy is estimated to be slightly higher than half the maximum energy value. The higher DQE values and the slightly different curve shape, as compared to those in Fig. 3, are explained by considering that, due to the spectrum of X-rays, the mean X-ray energy (in keV) is lower, e.g. approximately one half of the corresponding voltage value (in kVp). Fig. 5 displays DQE variation with coating thickness at two X-ray energies. For a given X-ray energy DQE increases with scintillator thickness while for a specific thickness DQE decreases with energy.

Curves and numerical values shown in Figs. 4 and 5 are similar to those obtained in previous studies, using either the Hamaker–Ludwig and Swank theoretical models or experimental techniques based on X-ray luminescence measurements (Cavouras et al., 1996, 1998, 2000; Kandarakis and Cavouras, 2001a,b). Using both experimental and

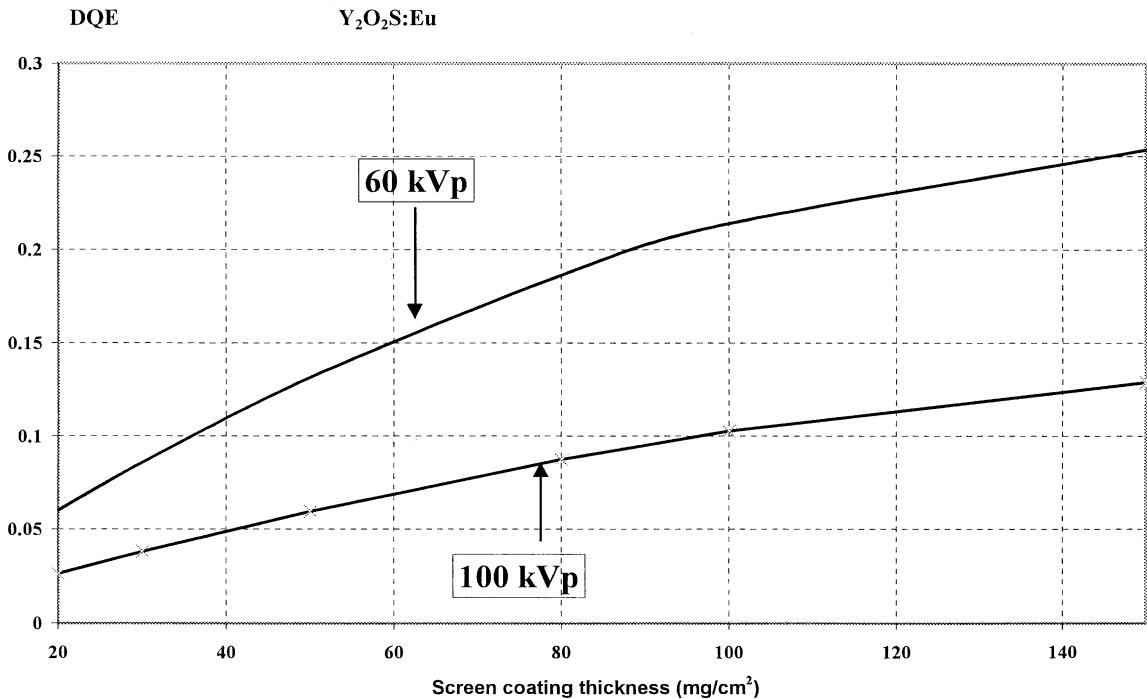


Fig. 5. Comparison of DQE curves determined at 60 and 100 kVp.

theoretical techniques, the DQE of $\text{La}_2\text{O}_2\text{S}:\text{Tb}$ at zero frequency has been previously found equal to 0.2 at 60 kVp for a 80 mg/cm^2 thick scintillator (Kandarakis and Cavouras, 2001b). This value is close enough to the value found in this study (see Fig. 4) at 60 kVp for a 100 mg/cm^2 thick scintillator. In addition values found by others (Dick and Motz, 1981; Ginzbourg and Dick, 1993) using photon counting techniques on commercial scintillating screens, are, in most cases, within the limits of $\text{DQE} = 0.2$ and $\text{DQE} = 0.4$ in the energy range from 50 to 60 keV, which is close to the mean energy of 100 kVp spectrum used in this work.

In conclusion the proposed theoretical model may give accurate results, however, this accuracy depends on the accuracy of the values fed as input data to the model. To apply this model in practical problems the following parameters should be known: (i) The values of the X-ray attenuation and absorption coefficients. These coefficients are functions of energy and should be calculated using tabulated data concerning the chemical elements in the scintillator for each energy value in the incident X-ray beam spectrum. To determine this spectrum, the type (aluminum, molybdenum or copper) and the thickness of the X-ray tube filter, the type of the tube's high voltage generator and the patient or phantom thickness and composition must be known. (ii) The values of the optical scattering and absorption coefficients used in the calculations. These coefficients should be either determined by model fitting on experimental data or by optical measurements. (iii) The value of the intrinsic X-ray to light conversion efficiency, which may be determined by methods similar to those of optical coefficients.

Acknowledgements

This study is dedicated to the memory of Professor G. E. Giakoumakis, leading member of our team, whose work on phosphor materials has inspired us to continue.

Appendix A

Following Eq. (6) in the text, $\bar{\Phi}_{A,B}^i(n, m)$ may be written as:

$$\Phi_{A,B}^i(n, m) = \Phi_{A,B}^i(0, m) \exp[-n(\lambda_A + \lambda_S) dL]. \quad (\text{A.1})$$

where the variance of $\bar{\Phi}_A$ is given by the well known relation:

$$\text{var}[\bar{\Phi}_A^X] = \overline{\Phi_A^{X^2}} - \bar{\Phi}_A^{X^2}. \quad (\text{B.3})$$

The first term of (B.3) is the average value of the squares of the optical quanta emitted from various depths in the scintillator and the second term is the square of the mean value of the same optical quanta. Considering Poisson statistical distribution for the absorbed X-ray quanta, the variance of Φ_Q is given as:

$$\text{var}[\Phi_Q^{\text{ABS}}] = \bar{\Phi}_Q^{\text{ABS}}. \quad (\text{B.4})$$

From (B.2), (B.3), (B.4) Eq. (B.2) may be written as:

$$\text{var}[\Phi_A] = \bar{\Phi}_Q^{\text{ABS}} \overline{\Phi_A^{X^2}}, \quad (\text{B.5})$$

which is Eq. (10) of the main text.

References

- Arnold, B.A., 1979. Physical characteristics of screen-film combinations. In: Haus, A.G. (Ed.), *The Physics of Medical Imaging: Recording System, Measurements and Techniques*. American Association of Physicists in Medicine, New York, pp. 30–71.
- Bunch, C.P., Huff, K.E., Van Metter, R., 1987. Analysis of the detective quantum efficiency of a radiographic screen-film combination. *J. Opt. Soc. Am. A* 4, 902.
- Cavouras, D., Kandarakis, I., Panayiotakis, G., Evangelou, E.K., Nomicos, C.D., 1996. An evaluation of the $\text{Y}_2\text{O}_3:\text{Eu}^{3+}$ scintillator for application in medical X-ray detectors and image receptors. *Med. Phys.* 23, 1965.
- Cavouras, D., Kandarakis, I., Panayiotakis, G.S., Kanellopoulos, E., Triantis, D., Nomicos, C.D., 1998. An investigation of the imaging characteristics of the $\text{Y}_2\text{O}_2\text{S}:\text{Eu}$ phosphor for application in X-ray detectors of digital mammography. *Appl. Radiat. Isot.* 49, 931.
- Cavouras, D., Kandarakis, I., Nomicos, C.D., Bakas, A., Panayiotakis, G.S., 2000. Measurement of the $(\text{Gd}, \text{La})_2\text{O}_2:\text{Tb}$ phosphor efficiency for X-ray imaging applications. *Radiat. Meas.* 32, 5.
- Curry, T.S., Dowdey, J.E., Murry, R.C., 1990. Luminescent Screens. In: *Christensen's Physics of Diagnostic Radiology*. Lea & Febiger, London, pp. 118–136.
- Dainty, J.C., Shaw, R., 1974. Detective quantum efficiency, signal to noise ratio, and the noise-equivalent number of quanta. In: *Image Science*, Academic Press, New York, pp. 152–188.
- Dick, C.E., Motz, J.W., 1981. Image information transfer properties of X-ray fluorescent screens. *Med. Phys.* 8, 337.
- Giakoumakis, G.E., Katsarioti, M.C., Lagaris, I.E., Panayiotakis, G.S., 1991. A theoretical model for the X-ray luminescence of granular phosphor screens. *J. Appl. Phys.* 69, 6607.
- Ginzbourg, A., Dick, C.E., 1993. Image information transfer properties of X-ray intensifying screens in the range from 17 to 320 keV. *Med. Phys.* 20, 1013.
- Gurvich, A.M., 1995. Luminescent screens for mammography. *Radiat. Meas.* 24, 325.
- Hamaker, H., 1947. Radiation and heat conduction in light-scattering material. *Philips Res. Rep.* 2, 55.
- Johns, H.E., Cunningham, J.R., 1983. *Diagnostic Radiology*. In: Thomas, C.C. (Ed.), *The Physics of Radiology*. Springfield, Illinois, pp. 557–669.
- Kandarakis, I., Cavouras, D., 2001a. Role of the activator in the performance of scintillators used in X-ray imaging. *Appl. Radiat. Isot.* 54, 821.
- Kandarakis, I., Cavouras, D., 2001b. Experimental and theoretical assessment of the performance of $\text{Gd}_2\text{O}_2\text{S}:\text{Tb}$ and $\text{La}_2\text{O}_2\text{S}:\text{Tb}$ phosphors and $\text{Gd}_2\text{O}_2\text{S}:\text{Tb}-\text{La}_2\text{O}_2\text{S}:\text{Tb}$ mixtures for X-ray imaging. *Eur. Radiol.* 11, 1083.
- Kandarakis, I., Cavouras, D., Panayiotakis, G., Agelis, T., Nomicos, C., Giakoumakis, G., 1996. X-ray induced luminescence and spatial resolution of $\text{La}_2\text{O}_2\text{S}:\text{Tb}$ phosphor screens. *Phys. Med. Biol.* 41, 297.
- Kandarakis, I., Cavouras, D., Panayiotakis, G.S., Nomicos, C.D., 1997a. Evaluating X-ray detectors for radiographic applications: a comparison of $\text{ZnSCdS}:\text{Ag}$ with $\text{Gd}_2\text{O}_2\text{S}:\text{Tb}$ and $\text{Y}_2\text{O}_2\text{S}:\text{Tb}$ screens. *Phys. Med. Biol.* 42, 1351.
- Kandarakis, I., Cavouras, D., Panayiotakis, G.S., Triantis, D., Nomicos, C.D., 1997b. An experimental method for the determination of spatial frequency dependent detective quantum efficiency (DQE) of scintillators used in X-ray imaging detectors. *Nucl. Instrum. Methods A* 399, 335.
- Kandarakis, I., Cavouras, D., Nomicos, C.D., Panayiotakis, G.S., 2001. X-ray luminescence of $\text{ZnSCdS}:\text{Au,Cu}$ phosphor using X-ray beams for medical applications. *Nucl. Instrum. Methods B* 179, 215.
- Kubelka, P., 1948. New contributions to the optics of intensely light-scattering materials. *J. Opt. Soc. Am.* 38, 448.
- Lindström, J., Carlsson, G.A., 1999. A simple model for estimating the particle size dependence of absolute efficiency of fluorescent screens. *Phys. Med. Biol.* 44, 1353.
- Ludwig, G.W., 1971. X-ray efficiency of powder phosphors. *J. Electrochem. Soc.* 118, 1152.
- Press, W.H., Flannery, B.P., Teukolsky, S.A., Vetterling, W.T., 1990. *Numerical Recipes in C: The Art of Scientific Computing*, Cambridge University Press, Cambridge, pp. 540–547.

- Sandborg, M., Carlsson, G.A., 1992. Influence of X-ray spectrum, contrasting detail and detector on the signal to noise ratio and detective quantum efficiency in projection radiography. *Phys. Med. Biol.* 33, 1245.
- Shaw, R., Van Metter, R., 1984. An analysis of the fundamental limitations of screen-film systems for X-ray detection. *Proc. SPIE* 454, 128.
- Storm, E., 1972. Calculated bremsstrahlung spectra from thick tungsten targets. *Phys. Rev. A* 5, 2328.
- Storm, E., Israel, H., 1967. Photon cross-sections from 0.001 to 100 MeV for elements 1 through 100 Report LA-3753 Los Alamos Scientific Laboratory of the University of California.
- Swank, R.K., 1972. Absorption and noise in X-ray phosphors. *J. Appl. Phys.* 44, 4199.
- Swank, R.K., 1973. Calculation of modulation transfer functions of X-ray fluorescent screens. *Appl. Opt.* 12, 1865.
- Tan, D., Heaton, B., 1994. Bremsstrahlung intensity and spectrum-theoretical deduction and discussion. *Appl. Radiat. Isot.* 45, 1101.
- Tucker, D.M., Barnes, G.T., Chakraborty, D.B., 1991. Semi-empirical model for generating tungsten target x-ray spectra. *Med. Phys.* 18, 211.
- Tapiovaara, M.J., Wagner, R.F., 1985. SNR and DQE analysis of broad spectrum X-ray imaging. *Phys. Med. Biol.* 30, 519.
- Williams, M.B., Simoni, P.U., Smilowitz, L., Stanton, M., Phillips, W., Stewart, A., 1999. Analysis of the detective quantum efficiency of a developmental detector for digital mammography. *Med. Phys.* 26, 2273.
- Yaffe, M.J., Rowlands, J.K., 1997. X-ray detectors for digital radiography. *Phys. Med. Biol.* 42, 1.
- Zweig, G., Zweig, D.A., 1983. Radioluminescent imaging: factors affecting total light output. *Proc. SPIE* 419, 297.